European Journal of Radiology 113 (2019) 238–244

Contents lists available at ScienceDirect

European Journal of Radiology

journal homepage: www.elsevier.com/locate/ejrad

Research article

Histogram analysis combined with morphological characteristics to discriminate adenocarcinoma in situ or minimally invasive adenocarcinoma from invasive adenocarcinoma appearing as pure ground-glass nodule

Teng Zhang[a], Xue-Hui Pu[a,1], Mei Yuan[a], Yan Zhong[a], Hai Li[b], Jiang-Fen Wu[c], Tong-Fu Yu[a,*]

[a] Department of Radiology, The First Affiliated Hospital of Nanjing Medical University, Nanjing, 210029, China
[b] Department of Pathology, The First Affiliated Hospital of Nanjing Medical University, Nanjing, 210029, China
[c] GE Healthcare, Shanghai, 200025, China

ARTICLE INFO

Keywords:
CT
Ground-glass nodule
Adenocarcinoma in situ
Minimally invasive adenocarcinoma
Histogram analysis

ABSTRACT

Objective: To construct a predictive model to discriminate adenocarcinoma in situ (AIS) or minimally invasive adenocarcinoma (MIA) from invasive adenocarcinoma (IAC) appearing as pure ground-glass nodules (pGGNs) using computed tomography (CT) histogram analysis combined with morphological characteristics and to evaluate its diagnostic performance.

Materials and methods: Two hundred eighty-nine patients with surgically resected solitary pGGN and pathologically diagnosed with AIS, MIA, or IAC in our institution from January 2014 to May 2018 were enrolled in our study. Two hundred twenty-six pGGNs (79 AIS, 84 MIA, and 63 IAC) were randomly selected and assigned to a model-development cohort, and the remaining 63 pGGNs (11 AIS, 29 MIA and 23 IAC) were assigned to a validation cohort. The morphological characteristics were established as model A and histogram parameters as model B. The diagnostic performances of model A, model B, and model A + B were evaluated and compared via receiver operating curve (ROC) analysis and logistic regression analysis.

Results: Entropy (odd ratio [OR] = 23.25, 95%CI: 6.83–79.15, $p < 0.001$), microvascular sign (OR = 8.62, 95%CI: 3.72–19.98, $p < 0.001$) and the maximum diameter (OR = 4.37, 95%CI: 2.44–7.84, $p < 0.001$) were identified as independent predictors in the IAC group. The area under the ROC (Az value), accuracy, sensitivity and specificity of model A + B were 0.896, 88.1%, 79.4% and 91.4%, respectively, exhibiting a significantly higher Az value than either model A or model B alone (0.785 vs 0.896, $p < 0.001$; 0.849 vs 0.896, $p = 0.029$). Model A + B also conveyed a good diagnostic performance in the validation cohort, with an Az value of 0.851.

Conclusion: Histogram analysis combined with morphological characteristics exhibit a superior diagnostic performance in discriminating AIS-MIA from IAC appearing as pGGNs.

1. Introduction

With the popularization of computed tomography (CT) screening for lung cancer in high-risk populations, the detection rate of pure ground-glass nodules (pGGNs) has significantly increased [1]. Persistent pGGNs lasting for more than three months have been proven to be highly associated with early-stage lung adenocarcinoma (LAC) [2]. According to the new classification proposed by IASLC/ATS/ERS in 2011, LAC is classified into pre-invasive lesions, including atypical adenomatous hyperplasia (AAH), adenocarcinoma in situ (AIS), minimally invasive adenocarcinoma (MIA) and invasive adenocarcinoma (IAC) [3]. Approximately 20% LACs manifest as pGGNs on CT images, the majority of which are pre-invasive lesions and MIAs, while only a few are IACs [4].

Wedge resection or segmentectomy is usually the surgical method implemented for AIS and MIA to maximize the preservation of functional pulmonary parenchyma. Following complete resection, 5-year survival stands at 100% or close to it [5]. Because there is no regional lymph node metastasis or distal metastasis in AIS and MIA, it is unnecessary to perform lymph node dissection during surgery. Lobectomy

* Corresponding author at: Department of Radiology, The First Affiliated Hospital of Nanjing Medical University, 300, Guangzhou Road, Nanjing, Jiangsu Province, 210029, China.
E-mail addresses: shenhua1004@163.com (T. Zhang), njmu_pxh@163.com (X.-H. Pu), 547816604@qq.com (M. Yuan), 1181449872@qq.com (Y. Zhong), 2414133362@qq.com (H. Li), jiangfenwu@ge.com (J.-F. Wu), njmu_ytf@163.com (T.-F. Yu).
[1] These authors contributed equally to this work.

https://doi.org/10.1016/j.ejrad.2019.02.034
Received 22 November 2018; Received in revised form 10 January 2019; Accepted 25 February 2019
0720-048X/ © 2019 Elsevier B.V. All rights reserved.

is usually chosen for IAC, for which lymph node dissection is required. The 5-year survival of IAC with pathological stage IA is 74.6% after complete resection [6]. Therefore, it is of great clinical significance to distinguish between AIS-MIA and IAC appearing as pGGNs in terms of surgical approaches and survival analysis.

Currently, the measured CT size and density represent key morphological parameters in determining the invasiveness of pGGNs. A study by Lim et al. [7] demonstrated that 16.4 mm was the optimal cut-off value for the maximum diameter to differentiate MIA from IAC, while the results from Han et al. indicated 17.2 mm as the cut-off [8]. Although the size of pGGN is positively correlated with the size and number of histopathological invasive foci, invasive foci may also occur in pGGNs smaller than 10 mm in size [9]. Zhou et al. [10] believe that -583.60 HU is the optimal cut-off value for tumor invasiveness in pGGNs. However, the increase in density of pGGNs may be associated with fibroblast proliferation or alveolar cavity collapse rather than the presence of invasive foci [11]. Therefore, it is difficult to differentiate AIS-MIA from IAC using only a visual CT assessment.

Texture analysis can be used to evaluate tumor heterogeneity and intrinsic invasiveness through analysis of the distribution and correlation of pixels or voxel gray scales in images, along with deep mining of their fine structures and the law of variations. Histogram analysis is the most commonly used method for texture analysis and it has been used to evaluate invasiveness in previous studies, but is primarily used for part-solid nodules and seldom in pGGNs [10,12,13]. Li et al. [14] found that the maximum nodule diameter and 100th percentile on CT number histogram were independent predictors for differentiating AAH-AIS from MIA-IAC appearing as pGGNs. However, because the 5-year survival of MIA after complete resection is close to 100%, we believe it is more clinically meaningful to assign it to the same category as AIS.

There have been no studies on combining the CT morphological parameters with histogram analysis to predict the invasiveness of pGGNs. Therefore, the purpose of our study was to combine these two methods to distinguish AIS-MIA from IAC and to evaluate its diagnostic performance, thereby providing guidance for the clinical management of pGGNs.

2. Materials and methods

2.1. Patients

This retrospective study was approved by the institutional review board with a waiver of written informed consent. From January 2014 to May 2018, 1162 GGNs from the surgical dataset pathologically diagnosed with AIS, MIA, or IAC in our institution were systematically reviewed and analyzed. Because AAH is usually less than 5 mm wide on imaging [15], we excluded AAHs from our study. Patients who met the following criteria were enrolled: (a) pGGNs without any solid component (excluding vessels and bronchi) observed with a lung window setting (window width, 1500 HU; window level, −600 HU; slice-thickness, 1.0 mm) on chest CT images; (b) maximum diameters of pGGNs between 5 mm and 3 cm; (c) non-enhanced thin-section CT scans performed within one week prior to surgery; (d) no therapeutic history before surgery; and (e) a definite pathological diagnoses based on surgical resection. Ultimately, 289 patients with solitary surgically resected pGGN pathologically diagnosed with AIS, MIA, or IAC were enrolled in our study. Two hundred twenty-six pGGNs (79 AIS, 84 MIA and 63 IAC) were randomly selected and assigned to a model-development cohort, and the remaining 63 pGGNs (11 AIS, 29 MIA and 23 IAC) were assigned to a validation cohort.

2.2. CT scanning

All patients underwent a non-enhanced thoracic CT scan with 128-slices (SOMATOM Definition AS+; Siemens, Malvern, PA, USA) CT scanner using the following settings: 1.0 mm slice-thickness and 0.8 mm reconstruction interval, 120 kVp and CareDose mAs for radiation reduction. All images were reconstructed using a high-kernel (b60) and high-resolution 512 × 512 matrix.

2.3. Imaging analysis

The entire-tumor volume of interest (VOI) was automatic segmented using MM oncology lungCAD software in Syngo.Via, Version VA30. The precise edges of the VOI were manually adjusted by thoracic radiologist (author two, who had four years' experience in thoracic imaging), if necessary to exclude normal vessels besides nodules as much as possible or when the borders of nodules were undefined. Then, author three and four who had 11 and 7 years' experience in thoracic imaging, rechecked the borders to ensure the accuracy of segmentation in consultation.

Histogram parameters, including entropy, kurtosis, maximum and mean CT value, skewness, uniformity, volume, variance and percentile CT numbers (10th, 50th, 90th percentiles), were extracted from segmented VOIs that were previously delineated using Analysis Kit software, Version 3.0 (GE Healthcare, Shanghai, China).

Two thoracic radiologists who rechecked the borders of VOI and were blinded to the pathologic diagnosis interpreted the CT images in consultation. The following CT morphological features were read with both lung (window width, 1500 HU; window level, −600 HU) and mediastinal (window width, 500 HU; window level, 50 HU) window settings: (1) diameter of pGGNs (maximal diameter on the axial section); (2) shapes (round/oval, irregular); (3) borders (defined, undefined); (4) vacuole sign (single or multiple cystic cavity with diameter < 5 mm were present within GGNs); (5) air bronchogram sign (air-filled bronchi seen within the GGNs); (6) microvascular sign (GGNs with dilated, convergent or tortuous supplying vessels); and (7) pleural indentation (linear attenuation heading toward the pleura or the major or minor fissure from GGNs). The image interpretation results were rechecked by author three to reach a consensus.

2.4. Pathological evaluation

Each surgically resected specimen was fixed in 10% formalin, embedded in paraffin, and stained with hematoxylin-eosin (H&E). Immunohistochemistry was performed if the histopathological classification under optical microscopy was equivocal. Elastic fiber staining was added to specimens in which it was necessary to assess pleural invasion. All specimens were classified by two experienced pathologists in consensus according to the 2011 IASLC/ATS/ERS lung adenocarcinoma classification criteria.

2.5. Statistical analysis

Continuous variables were compared by Student's *t*-test or the Mann-Whitney U test according to whether the data conformed to a normal distribution. Differences in categorical variables were analyzed using Pearson's chi-square test and Fisher's exact test.

Variables that exhibited statistically significant differences in the model-development cohort were included in multivariate logistic regression analysis. The established predictive model and its diagnostic performance in the validation cohort were analyzed using receiver operating characteristic (ROC) regression analysis. The diagnostic sensitivity, specificity, accuracy and area under the ROC curve (AUC) were calculated at a cut-off value in context of the maximum Youden index. ROC curves were compared and estimated using MedCalc statistical software (version 8.2.0.1, MedCalc Software, Mariakerke, Belgium). The Akaike information criterion (AIC) in χ^2 analysis was used to determine the best-fit model.

P-values < 0.05 were considered statistically significant. All statistical analyses were performed using IBM SPSS Statistics, version 22.0 (SPSS, Inc., Chicago, Ill., USA).

Table 1
Clinical and morphological characteristics of the model-development and validation cohorts.

Characteristics	Overall cohort (n = 289)	Model-development cohort (n = 226)	Validation cohort (n = 63)	P value
Age (year)	54.70 ± 10.62	55.28 ± 10.82	52.62 ± 9.69	0.078[a]
Sex (Male/Female)	86 (29.8) /203 (70.2)	61 (27.0) /165 (73.0)	20 (31.7) /43 (68.3)	0.457[b]
Smoking history (Yes/No)	42 (14.5) /247 (85.5)	30 (13.3) /196 (86.7)	12 (19.0) /51 (81.0)	0.250[b]
Lesion location				0.680[b]
Right upper lobe	118 (40.8)	88 (38.9)	30 (47.6)	
Right middle lobe	27 (9.3)	22 (9.7)	5 (7.9)	
Right lower lobe	35 (12.1)	30 (13.3)	5 (7.9)	
Left upper lobe	74 (25.6)	58 (25.7)	16 (25.4)	
Left lower lobe	35 (12.1)	28 (12.4)	7 (11.1)	
Maximum diameter (cm)	1.08 ± 0.44	1.08 ± 0.45	1.09 ± 0.42	0.596[c]
Lesion shape				0.345[b]
Round/Oval	228 (78.9)	181 (80.1)	47 (74.6)	
Irregular	61 (21.1)	45 (19.9)	16 (25.4)	
Lesion border				0.889[b]
Defined	209 (72.3)	163 (72.1)	46 (73.0)	
Undefined	80 (27.7)	63 (27.9)	17 (27.0)	
Vacuole sign (Yes/No)	37 (12.8) /252 (87.2)	30 (13.3) /196 (86.7)	7 (11.1) /56 (88.9)	0.650[b]
Air bronchogram (Yes/No)	23 (8.0) /266 (92.0)	17 (7.5) /209 (92.5)	6 (9.5) /57 (90.5)	0.604[b]
Microvascular sign (Yes/No)	72 (24.9) /217 (75.1)	52 (23.0) /174 (77.0)	20 (31.7) /43 (68.3)	0.156[b]
Pleural indentation (Yes/No)	43 (14.9) /246 (85.1)	31 (13.7) /195 (86.3)	12 (19.0) /51 (81.0)	0.293[b]
Pathological classification				0.185[b]
AIS-MIA group	203 (70.2)	163 (72.1)	40 (63.5)	
AIS	90	79	11	
MIA	113	84	29	
IAC group	86 (29.8)	63 (27.9)	23 (36.5)	
Lepidic adenocarcinoma	56	40	16	
Acinar adenocarcinoma	28	21	7	
Papillary adenocarcinoma	2	2	0	

Note. -Values are presented as no. (%) or mean ± standard deviation.
AIS = adenocarcinoma in situ; MIA = minimally invasive adenocarcinoma; IAC = invasive adenocarcinoma.
[a] Student's *t*-test.
[b] Pearson's chi-square test and Fisher's exact test.
[c] Mann-Whitney U test.

Table 2
Comparison of the clinical and morphological characteristics between the AIS-MIA group and IAC group in the model-development cohort.

Characteristics	Model-development cohort (n = 226)	AIS-MIA group (n = 163)	IAC group (n = 63)	P value
Age (year)	55.28 ± 10.82	54.12 ± 10.28	58.13 ± 11.64	0.012[a]
Sex (Male/Female)	61 (27.0) /165 (73.0)	43 (26.4) /120 (73.6)	18 (28.6) /45 (71.4)	0.739[b]
Smoking history (Yes/No)	30 (13.3) /196 (86.7)	23 (14.1) /140 (85.9)	7 (11.1) /56 (88.9)	0.551[b]
Lesion location				0.431[b]
Right upper lobe	88 (38.9)	62 (38.1)	26 (41.3)	
Right middle lobe	22 (9.7)	18 (11.0)	4 (6.4)	
Right lower lobe	30 (13.3)	18 (11.0)	12 (19.0)	
Left upper lobe	58 (25.7)	44 (27.0)	14 (22.2)	
Left lower lobe	28 (12.4)	21 (12.9)	7 (11.1)	
Maximum diameter (cm)	1.08 ± 0.45	0.98 ± 0.36	1.32 ± 0.54	0.000[c]
Lesion shape				0.000[b]
Round/Oval	181 (80.1)	145 (89.0)	36 (57.1)	
Irregular	45 (19.9)	18 (11.0)	27 (42.9)	
Lesion border				0.885[b]
Defined	163 (72.1)	118 (72.4)	45 (71.4)	
Undefined	63 (27.9)	45 (27.6)	18 (28.6)	
Vacuole sign (Yes/No)	30 (13.3) /196 (86.7)	16 (9.8) /147 (90.2)	14 (22.2) /49 (77.8)	0.014[b]
Air bronchogram (Yes/No)	17 (7.5) /209 (92.5)	6 (3.7) /157 (96.3)	11 (17.5) /52 (82.5)	0.000[b]
Microvascular sign (Yes/No)	52 (23.0) /174 (77.0)	20 (12.3) /143 (87.7)	32 (50.8) /31 (49.2)	0.000[b]
Pleural indentation (Yes/No)	31 (13.7) /195 (86.3)	17 (10.4) /146 (89.6)	14 (22.2) /49 (77.8)	0.021[b]

Note. -Values are presented as no. (%) or mean ± standard deviation.
AIS = adenocarcinoma in situ; MIA = minimally invasive adenocarcinoma; IAC = invasive adenocarcinoma.
[a] Student's *t*-test.
[b] Pearson's chi-square test and Fisher's exact test.
[c] Mann-Whitney U test.

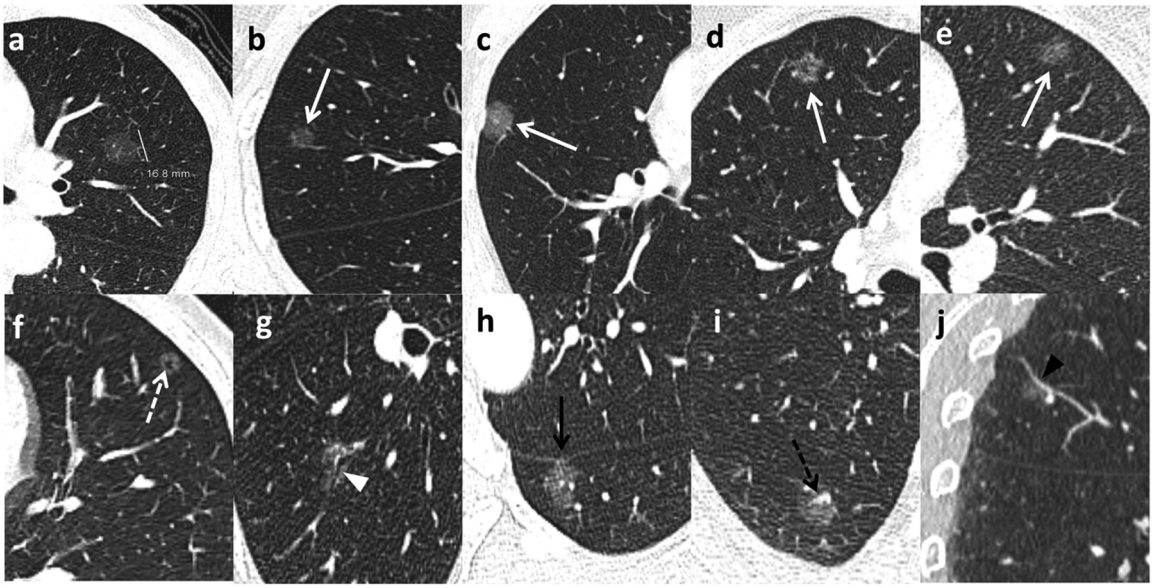

Fig. 1. For the 289 pGGNs included in our study, thin-section CT morphological characteristics were evaluated. (a) The maximal diameter of the nodule is measured on the axial lung window image. The nodule shape is evaluated as (b) round, (c) oval, or (d) irregular. The nodule border is evaluated as (b), (c), (d) defined, and (e) undefined. (f) A 45-year-old man with AIS in the left upper lobe exhibits a bubble-like lucency within the nodule (white dotted arrow). (g) A 70-year-old woman with MIA in the right lower lobe shows air-filled bronchi present inside the lesion (white arrowhead). (h) A 47-year-old woman with MIA shows a lesion with pleural indentation in the left lower lobe adjacent to the oblique fissure (black arrow). (i, *j*) A 62-year-old woman with IAC in the right upper lobe. The microvascular sign is demonstrated as a small adjacent pulmonary vessel entering the lesion (black dotted arrow). Reverse tracing shows that the blood vessel is a branch of the pulmonary artery. Coronal reconstruction better shows the dilation of the supplying vessel (black arrowhead).

Table 3
Univariate analysis of the histogram parameters in the model-development cohort.

Characteristics	AIS-MIA group (n = 163)	IAC group (n = 63)	P value
Entropy	3.17 ± 0.37	3.57 ± 0.34	0.000[a]
Kurtosis	5.18 ± 3.28	5.09 ± 2.10	0.208[b]
Skewness	0.97 ± 0.68	1.08 ± 0.49	0.040[b]
Uniformity	0.14 ± 0.03	0.10 ± 0.02	0.000[b]
Variance	28898.19 ± 21838.37	49464.25 ± 27080.27	0.000[b]
Volume (ml)	0.88 ± 0.54	1.26 ± 1.16	0.000[b]
Mean CT value (HU)	−681.82 ± 88.96	−594.64 ± 98.53	0.000[b]
Maximum CT value (HU)	−126.26 ± 92.38	−29.61 ± 86.23	0.000[b]
10th percentile (HU)	−861.37 ± 54.22	−829.57 ± 56.83	0.000[b]
50th percentile (HU)	−702.65 ± 81.49	−625.81 ± 88.92	0.000[b]
90th percentile (HU)	−480.96 ± 152.81	−325.46 ± 172.86	0.000[b]

Note. -Values are presented as no. (%) or mean ± standard deviation.
HU = Hounsfield unit; AIS = adenocarcinoma in situ; MIA = minimally invasive adenocarcinoma; IAC = invasive adenocarcinoma.
[a] Student's *t*-test.
[b] Mann-Whitney U test.

3. Results

3.1. Clinical and morphological characteristics of pGGNs

Two hundred eighty-nine patients (86 men, mean age 54.95 ± 9.88 years; 203 women, mean age 54.60 ± 10.95 years) with solitary pGGN (90 AIS, 113 MIA and 86 IAC) were enrolled in this study. The characteristics of both the model-development and validation cohorts are summarized in Table 1.

In the model-development cohort, 226 pGGNs were divided into two groups: 163 (72.1%) pGGNs, including 79 AIS and 84 MIA, were assigned to the AIS-MIA group, and 63 (27.9%) IAC were assigned to IAC group. Compared with the AIS-MIA group, patients with IAC were older (58.13 ± 11.64 vs 54.12 ± 10.28, p = 0.012) and exhibited tumors with larger diameters (1.32 ± 0.54 vs 0.98 ± 0.36, p < 0.001) and more irregular shapes (42.9% vs 11.0%, p < 0.001). The presence of the vacuole sign (p = 0.014), air bronchogram sign (p < 0.001), microvascular sign (p < 0.001) and pleural indentation (p = 0.021) were significantly associated with the extent of invasion. Table 2 and Fig. 1 present comparisons of the clinical and CT morphological characteristics between AIS-MIA and IAC groups.

3.2. Histogram analysis of pGGNs

In univariate analysis, histogram parameters, including entropy, maximum and mean CT values, skewness, uniformity, volume and percentile CT numbers (10th, 50th, 90th percentiles), were significantly different between the AIS-MIA and IAC groups in the model-development cohort. The details are illustrated in Table 3 and Fig. 2.

3.3. Multivariate logistic regression analysis

For multivariate analysis, we used all of clinical/morphological characteristics and histogram parameters that were statistically significant in the univariate analysis. The results revealed that entropy (odd ratio [OR] = 23.25, 95%CI: 6.83–79.15, p < 0.001), the microvascular sign (OR = 8.62, 95%CI: 3.72–19.98, p < 0.001) and the maximum diameter (OR = 4.37, 95%CI: 2.44–7.84, p < 0.001) were independent predictors for the IAC group (Table 4).

3.4. Construction and validation of the predictive model

The prediction factors for the probability of IAC in the model were generated as follows:

$$P = e^x/(1 + e^x)$$

where x = −13.60 + (3.146 × entropy) + (2.154 × microvascular sign) + (1.475 × maximum diameter) and e is the natural logarithm.

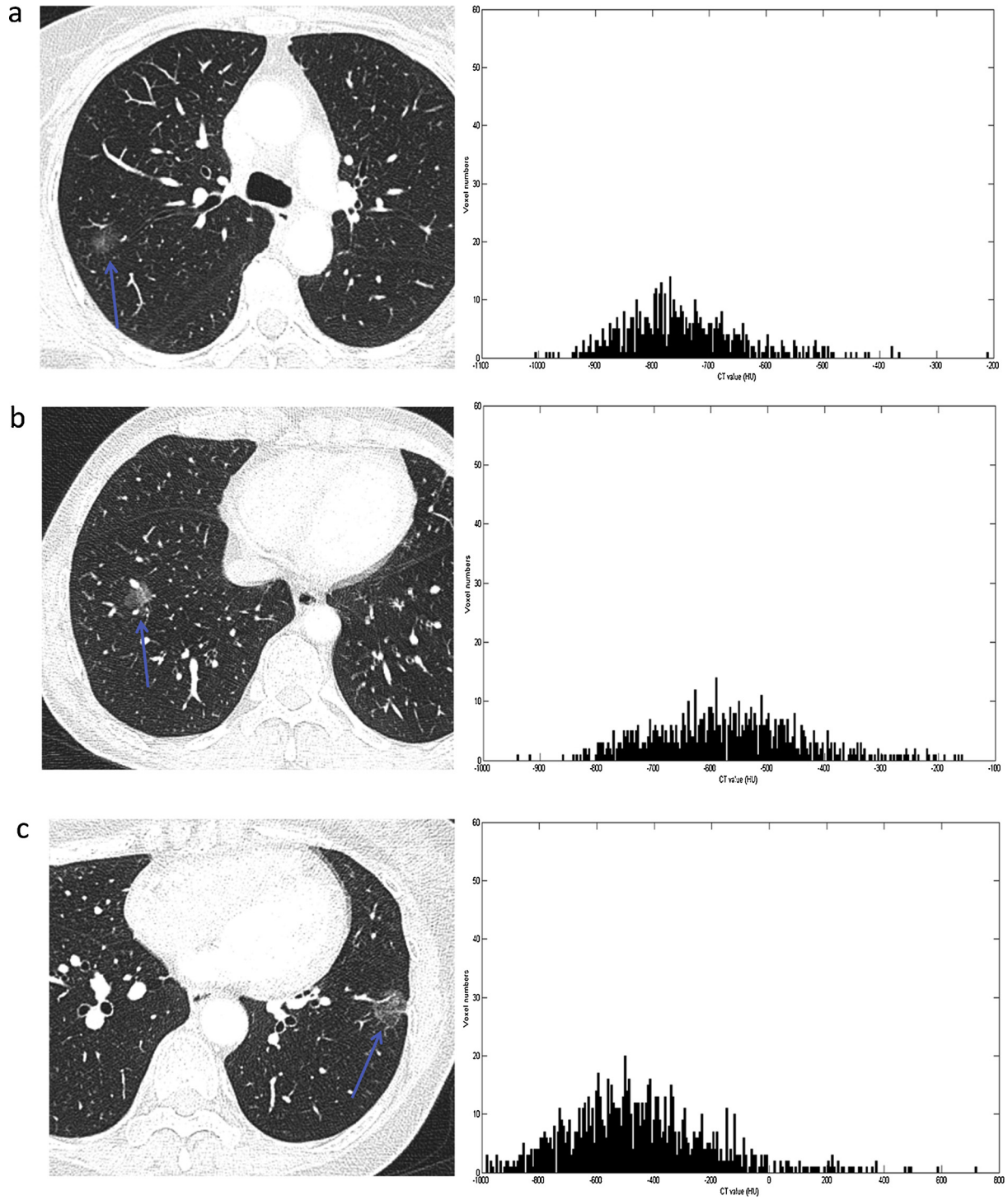

Fig. 2. CT images shown as a histogram distribution of CT values for pGGNs. If the value of entropy is high, then the distribution is among more intensity levels in the image and the pGGNs are more likely to be IAC. (a) A 53-year-old woman with AIS in the right upper lobe of the lung. The entropy value for the case was 2.89, which was lower than the cut-off value (3.29) in this study. (b) A 48-year-old man with MIA in the right lower lobe of the lung. The entropy value for the case was 3.12, which was lower than the cut-off value (3.29) in this study. (c) A 62-year-old woman with IAC in the left lower lobe of the lung. The entropy value for the case was 3.79, which was higher than the cut-off value (3.29) in this study.

The presence of a microvascular sign is scored as 1 or as 0 based on an assessment of the CT images.

The area under the ROC curve (Az value), accuracy, sensitivity and specificity of the predictive model were 0.896, 88.1%, 79.4%, and 91.4%, respectively, showing a significantly higher Az value than model A based on the clinical and morphological characteristics and model B based on the histogram parameters (0.896 vs 0.785, $p < 0.001$; 0.896 vs 0.849, $p = 0.029$). The predictive performance of model A + B was also significantly improved over those of model A and model B with respect to the model fit (AIC value 67.7% vs. 44.6%, 59.7%) (Fig. 3a, Table 5).

The parameters, including entropy, the microvascular sign and the maximum diameter measured and assessed, of the validation cohort were entered into the formula mentioned above, and the probability of

Table 4
Independent predictors in the multivariate logistic regression analyses and the odds ratios (ORs).

Factor	Regression coefficient	Standard error	P value	Odds ratio (95% confidence interval)
Entropy	3.146	0.625	0.000	23.25 (6.83–79.15)
Microvascular sign	2.154	0.429	0.000	8.62 (3.72–19.98)
Maximum diameter	1.475	0.298	0.000	4.37 (2.44–7.84)
Constant	−13.598	0.383	0.000	0.000

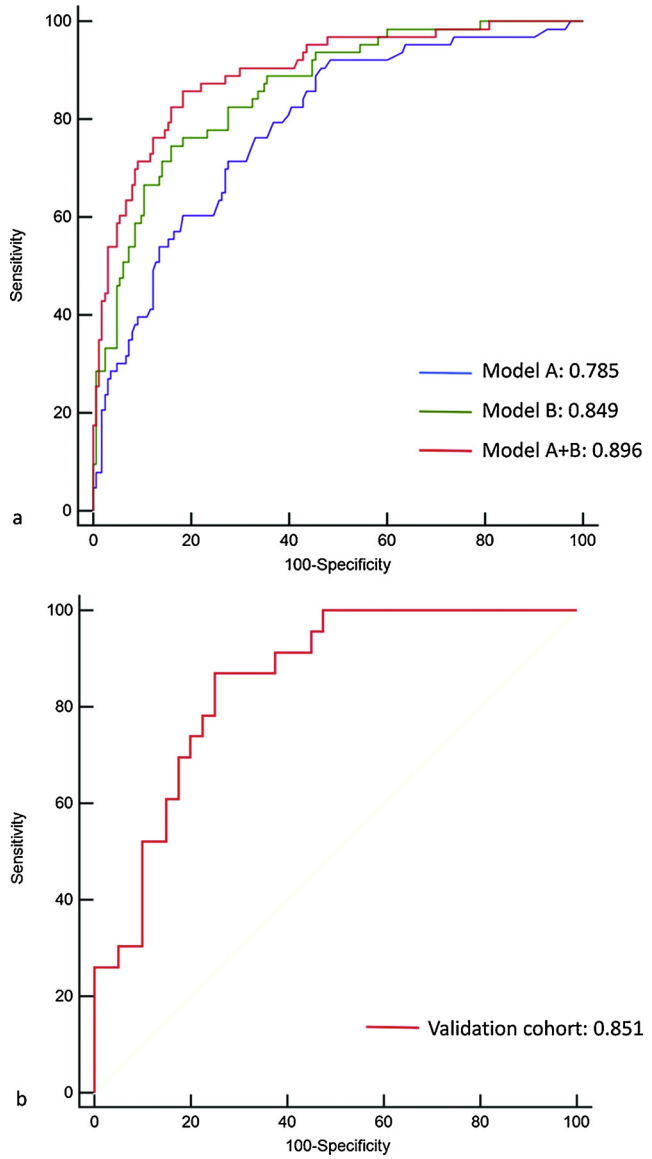

Fig. 3. (a) ROC analysis of model A, model B, and model A + B for distinguishing AIS-MIA from IAC. (b) ROC analysis of the validation cohort to evaluate the diagnostic performance of model A + B.

IAC was calculated. ROC analysis demonstrated that the constructed predictive model conveyed a good diagnostic performance in the validation cohort with an Az value of 0.851 (Fig. 3b).

4. Discussion

In 2011, IASLC/ATS/ERS proposed new classification for lung adenocarcinoma. However, uncertainty and ambiguity remain regarding this classification, particularly on pGGNs, in terms of the invasive extent [16]. In our study, a series of morphological characteristics were firstly analyzed and generated as model A for differentiating AIS-MIA from IAC. Consistent with previous studies [17–20], we found that IAC occurred more often in older patients, the presence of vacuoles, air bronchograms and pleural indentations were more frequently observed in IAC than in AIS-MIA. An irregular shape also significantly favored a diagnosis of IAC. But all these morphological characteristics were not the independent predictors for IAC group and the diagnostic performances of model A were also not desirable with Az value, accuracy of only 0.785, 80.5%.

Our study extends histogram analysis to discriminate AIS-MIA from IAC appearing as pGGNs. We demonstrate that histogram parameters combined with morphological characteristics exhibits a superior diagnostic performance, with an Az value, accuracy, sensitivity and specificity of 0.896, 88.1%, 79.4% and 91.4%, respectively. Entropy, microvascular sign and the maximum diameter were identified as independent predictors in the IAC group.

A previous study demonstrated that with the increase in invasiveness of lung adenocarcinoma observed in GGN, the lesion size increased accordingly [18]. In the current study, the maximum diameter was shown to be an independent factor in discriminating IAC. Heidinger et al. [9] reported a similar finding wherein measuring the nodule volume and the attenuation of pGGNs had no advantage over the average diameter measurement. pGGNs of greater than 16.4 mm maximum diameter have been reported to histopathologically represent invasive adenocarcinoma [7]. Lee et al. [16] indicated that when GGNs were 15 mm or more in diameter, nodules were more likely to be invasive adenocarcinomas. In our study, 11.6 mm was the best cut-off value to differentiate AIS-MIA from IAC, much lower than previous research has suggested. The most likely explanation is that although we have excluded AAHs from our study, the AIS-MIA group still occupies a large proportion of the model-development cohort (163 vs 63) because of the rarity of IAC appearing as pGGNs. Thus, these results require further validation with a larger sample size.

Sustained angiogenesis or vasculature remodeling is one of the initiating events occurring in the early stages of tumor development, as has been demonstrated by tumor biology studies [21]. Many studies have also demonstrated that the relationships between solid pulmonary nodules (SPNs) and vessels, especially the vascular convergence sign (VCS), are valuable for estimating the malignant potential of SPNs [22]. In our study, we revealed that the microvascular sign is a useful independent predictor for discriminating AIS-MIA from IAC, which is consistent with the study of Wu et al [18]. They included sub-centimeter pGGN adenocarcinoma and demonstrated that vessel changes within the GGN were earlier and more accurate in reflecting the histopathologic process, with vessel changes occurring in 53.3% of IAC, which was highly consistent with our results (32/63, 50.8%).

As pGGNs evolve and grow, invasive components containing structural deformities of the stromal elastic fiber framework appear within a homogeneous lepidic or acinar background, although they are difficult to observe by the naked eye due to the limited resolution (200–300 u m) of HRCT images, in which pixel values are expected to become inhomogeneous as invasive components increase in extent. In our study, we applied texture analysis to evaluate the invasiveness of pGGNs, demonstrating that entropy is an independent predictor for discriminating AIS-MIA from IAC, which was consistent with the findings of Hwang et al. [23]. Entropy measures the randomness of the distribution of coefficient values over the intensity levels [24]. If the

Table 5
Effectiveness of model A, model B and model A + B in discriminating AIS-MIA from IAC appearing as pGGNs.

Model development cohort	AIS-MIA (n = 163)	IAC (n = 63)	P value	Cut-off value	Accuracy (%)	Az	SEN (%)	SPE (%)	Model-fitting information	
									AIC (%)	R^2 value
Model A	0.22 ± 0.16	0.43 ± 0.24	0.000	> 0.157	80.5	0.785	57.1	89.6	44.6	0.195
Model B	0.18 ± 0.19	0.53 ± 0.28	0.000	> 0.356	83.6	0.849	61.9	92.0	59.7	0.354
Model A + B	0.15 ± 0.20	0.66 ± 0.26	0.000	> 0.270	88.1	0.896	79.4	91.4	67.7	0.456
Entropy	3.17 ± 0.37	3.57 ± 0.34	0.000	> 3.291		0.778	71.8	65.0		
Microvascular sign (Yes/No)	20 (12.3) /143 (87.7)	32 (50.8) /31 (49.2)	0.000	> 0		0.693	50.8	87.7		
Maximum diameter	0.98 ± 0.36	1.32 ± 0.54	0.000	> 1.16		0.710	77.8	56.4		

Note. - Az = area under the receiver operating curve; SEN = sensitivity; SPE = specificity; AIC = Akaike information criterion.

value of entropy is high, then the distribution is spread over more intensity levels in the image and the pGGNs are more likely to be IAC. In previous studies, entropy has been applied to evaluate the invasiveness of part-solid nodules, but has seldom been employed in pGGNs. Son et al. [25] reviewed 191 resected ground glass opacity nodules with little or no solid component and identified entropy as an independent predictor for invasive adenocarcinoma, which verifies our results to some extent.

There are some limitations in our study. First, this was a retrospective study with a relatively small sample size, especially with respect to the number of IAC cases, which was far fewer compared to that of AIS-MIA cases. More samples are needed in order to further improve and perfect our research. Second, sometimes the size measurement of pGGNs was difficult, especially lesions with unclear tumour-lung interface. Finally, the CT scans evaluated in our research were unenhanced, and we are unsure whether contrast enhanced CT will affect the measurement of pGGNs. Hence, to avoid indetermination, we excluded patients who underwent contrast enhanced CT. In a study by Kim et al. [26], it was demonstrated that the correlation between volumetric measurements and the invasive component size was moderate in non-enhanced CT scans and weak in contrast-enhanced CT scans. Further study is needed to compare the results of non-enhanced CT and contrast enhanced CT to evaluate the impact of contrast enhanced CT on the analytic results of pGGNs.

5. Conclusion

We found that histogram parameters combined with an evaluation of morphological characteristics exhibited a good diagnostic performance in discriminating AIS-MIA from IAC appearing as pGGNs, which will be helpful to guide the clinical diagnosis and management for the patients with pGGNs which were considered as high risk of malignancy.

Conflict of interest

All the authors have no conflicts of interest to disclose.

Role of the funding source

This research did not receive any specific grant from funding agencies in the public, commercial, or not-for-profit sectors.

References

[1] H. Matsuguma, K. Mori, R. Nakahara, et al., Characteristics of subsolid pulmonary nodules showing growth during follow-up with CT scanning, Chest 143 (2) (2013) 436–443.
[2] B. Chang, J.H. Hwang, Y.H. Choi, et al., Natural history of pure ground-glass opacity lung nodules detected by low-dose CT scan, Chest 143 (1) (2013) 172–178.
[3] W.D. Travis, E. Brambilla, M. Noguchi, et al., International Association for the Study of Lung Cancer/American Thoracic Society/European Respiratory Society international multidisciplinary classification of lung adencarcinoma, J. Thorac. Oncol. 6 (2) (2011) 244–285.
[4] C.I. Henschke, D.F. Yankelevitz, R. Mirtcheva, G. McGuinness, D. McCauley, O.S. Miettinen, CT screening for lung cancer: frequency and significance of part-solid and nonsolid nodules, AJR Am. J. Roentgenol. 178 (5) (2002) 1053–1057.
[5] S. Liu, R. Wang, Y. Zhang, et al., Precise diagnosis of intraoperative frozen section is an effective method to guide resection strategy for peripheral small-sized lung adenocarcinoma, J. Clin. Oncol. 34 (4) (2016) 307–313.
[6] J. Zhang, J. Wu, Q. Tan, L. Zhu, W. Gao, Why do pathological stage IA lung adenocarcinomas vary from prognosis?: a clinicopathologic study of 176 patients with pathological stage IA lung adenocarcinoma based on the IASLC/ATS/ERS classification, J. Thorac. Oncol. 8 (9) (2013) 1196–1202.
[7] H.J. Lim, S. Ahn, K.S. Lee, et al., Persistent pure ground-glass opacity lung nodules ≥10 mm in diameter at CT scan: histopathologic comparisons and prognostic implications, Chest 144 (4) (2013) 1291–1299.
[8] L. Han, P. Zhang, Y. Wang, et al., CT quantitative parameters to predict the invasiveness of lung pure ground-glass nodules (pGGNs), Clin. Radiol. 73 (5) (2018) 504.e1-504.e7.
[9] B.H. Heidinger, K.R. Anderson, U. Nemec, et al., Lung adenocarcinoma manifesting as pure ground-glass nodules: correlating CT size, volume, density, and roundness with histopathologic invasion and size, J. Thorac. Oncol. 12 (8) (2017) 1288–1298.
[10] Q.J. Zhou, Z.C. Zheng, Y.Q. Zhu, et al., Tumor invasiveness defined by IASLC/ATS/ERS classification of ground-glass nodules can be predicted by quantitative CT parameters, J. Thorac. Dis. 9 (5) (2017) 1190–1200.
[11] R. Kakinuma, M. Noguchi, K. Ashizawa, et al., Natural history of pulmonary subsolid nodules: a prospective multicenter study, J. Thorac. Oncol. 11 (7) (2016) 1012–1028.
[12] J.P. Ko, J. Suh, O. Ibidapo, et al., Lung adenocarcinoma: correlation of quantitative CT findings with pathologic findings, Radiology 280 (3) (2016) 931–939.
[13] M. Yuan, Y.D. Zhang, X.H. Pu, et al., Comparison of a radiomic biomarker with volumetric analysis for decoding tumour phenotypes of lung adenocarcinoma with different disease-specific survival, Eur. Radiol. 27 (11) (2017) 4857–4865.
[14] Q. Li, L. Fan, E.T. Cao, Q.C. Li, Y.F. Gu, S.Y. Liu, Quantitative CT analysis of pulmonary pure ground-glass nodule predicts histological invasiveness, Eur. J. Radiol. 89 (4) (2017) 67–71.
[15] X. Pan, X. Yang, J. Li, X. Dong, J. He, Y. Guan, Is a 5-mm diameter an appropriate cut-off value for the diagnosis of atypical adenomatous hyperplasia and adenocarcinoma in situ on chest computed tomography and pathological examination? J. Thorac. Dis. 10 (Suppl. 7) (2018) S790–S796.
[16] H.Y. Lee, Y. La Choi, K.S. Lee, et al., Pure ground-glass opacity neoplastic lung nodules: histopathology, imaging, management, AJR Am. J. Roentgenol. 202 (3) (2014) W224–233.
[17] Y. Liu, H. Sun, F. Zhou, et al., Imaging features of TSCT predict the classification of pulmonary preinvasive lesion, minimally and invasive adenocarcinoma presented as ground glass nodules, Lung Cancer 108 (6) (2017) 192–197.
[18] F. Wu, S. ping Tian, X. Jin, et al., CT and histopathologic characteristics of lung adenocarcinoma with pure ground-glass nodules 10 mm or less in diameter, Eur. Radiol. 27 (10) (2017) 4037–4043.
[19] X. Yue, S. Liu, S. Liu, et al., HRCT morphological characteristics distinguishing minimally invasive pulmonary adenocarcinoma from invasive pulmonary adenocarcinoma appearing as subsolid nodules with a diameter of ≤3 cm, Clin. Radiol. 73 (4) (2017) 411.e7-411.e15.
[20] Y.L. She, L.L. Zhao, L.C.Y. Dai, et al., Preoperative nomogram for identifying invasive pulmonary adenocarcinoma in patients with pure ground-glass nodule: a multi-institutional study, Oncotarget 8 (10) (2017) 17229–17238.
[21] D. Hanahan, R.A. Weinberg, Hallmarks of cancer: the next generation, Cell 144 (3) (2011) 646–674.
[22] F. Gao, M. Li, X. Ge, et al., Multi-detector spiral CT study of the relationships between pulmonary ground-glass nodules and blood vessels, Eur. Radiol. 23 (12) (2013) 3271–3277.
[23] I.P. Hwang, C.M. Park, S.J. Park, et al., Persistent pure ground-glass nodules larger than 5 mm: differentiation of invasive pulmonary adenocarcinomas from preinvasive lesions or minimally invasive adenocarcinomas using texture analysis, Invest. Radiol. 50 (11) (2015) 798–804.
[24] F. Davnall, C.S.P. Yip, G. Ljungqvist, et al., Assessment of tumor heterogeneity: an emerging imaging tool for clinical practice? Insights Imaging 3 (6) (2012) 573–589.
[25] J.Y. Son, H.Y. Lee, K.S. Lee, et al., Quantitative CT analysis of pulmonary ground-glass opacity nodules for the distinction of invasive adenocarcinoma from pre-invasive or minimally invasive adenocarcinoma, PLoS One 9 (8) (2014) e104066.
[26] H. Kim, J.M. Goo, C.M. Park, Evaluation of T categories for pure ground-glass nodules with semi-automatic volumetry: is mass a better predictor of invasive part size than other volumetric parameters? Eur. Radiol. 28 (10) (2018) 4288–4295.